Interdecadal Variation of the Transition Zone Chlorophyll Front, A Physical-Biological Model Simulation between 1960 and 1990

F. Chai[1], M. Jiang[1], R. T. Barber[2], R. C. Dugdale[3], and Y. Chao[4]

[1]School of Marine Science, 5471 Libby Hall, University of Maine, Orono, ME 04469-5741, USA

[2]Duke University, NSOE Marine Laboratory, 135 Duke Marine Lab Road, Beaufort, NC 28516, USA

[3]Romberg Tiburon Center, San Francisco State University, PO Box 855, Tiburon CA 94920, USA

[4]Jet Propulsion Laboratory, California Institute of Technology, 4800 Oak Grove Drive, Pasadena, CA 91109, USA

fchai@maine.edu

In press, *Journal of Oceanography,* August 2003

Abstract

The North Pacific Transition Zone (NPTZ) is bounded by two oceanographic fronts at approximately 30-32^{o}N (Subtropical Front) and 42-45^{o}N (Subarctic Front) in the central Pacific. The Transition Zone Chlorophyll Front (TZCF) is a biological front within the NPTZ that separates the low chlorophyll subtropical gyres and the high chlorophyll subarctic gyres in the central Pacific Ocean. The interdecadal climate variability affects marine ecosystems in both the subtropical and subarctic gyres, consequently the position of the TZCF. A three-dimensional physical-biological model has been used to study interdecadal variation of the TZCF using a retrospective analysis of a 30-year (1960-1990) model simulation. The physical-biological model is forced with the monthly mean heat flux and surface wind stress from the Comprehensive Ocean Atmosphere Data Set (COADS).

The modeled TZCF, operationally defined as the isopleth of 0.2 mg/m^3 surface chlorophyll, is located between 26^{o}N and 27^{o}N in the central North Pacific during the winter and between 34^{o}N and 35^{o}N during the summer, which agrees with the seasonal migration patterns of the TZCF detected with the SeaWiFS surface chlorophyll. The modeled winter mixed layer depth (MLD) shows the largest increase between 30^{o}N and 40^{o}N in the central North Pacific (150^{o}E to 180^o), with a value of 40-60% higher (deeper mixed layer) during 1979-90 relative to 1964-75 values. In the subarctic gyre in both the northeast (Ocean Station Papa) and northwest Pacific (Oyashio region), the modeled winter MLD decreases by about 20% during the period of 1979-90 relative to 1964-75 levels. The winter Ekman pumping velocity difference between 1979-90 and 1964-75 shows the largest increase located between 30^{o}N and 45^{o}N in the central and eastern North Pacific (180^o to 150^{o}W). In the subarctic northeast Pacific region including the

Gulf of Alaska, The winter Ekman pumping velocity decreases during the period of 1979-90, but its value increases in the northwest Pacific (Oyashio region) after the 1976-77 climatic shift. The modeled winter surface nitrate difference between 1979-90 and 1964-75 shows increase in the latitudinal band between 30^{o}N and 45^{o}N from the west to the east (135^{o}E-135^{o}W), the modeled nitrate concentration is about 10 to 50% higher in general during the period of 1979-90 relative to 1964-75 values depending upon locations. The increase in the winter surface nitrate concentration during 1979-90 is caused by a combination of the winter MLD increase and the winter Ekman pumping enhancement after the 1976-77 climatic shift. The modeled nitrate concentration increase after 1976-77 lead to the primary productivity increase in the central North Pacific (30^{o}N-40^{o}N and 180^{o}-140^{o}W). Enhanced primary productivity after the 1976-77 climatic shift contributes higher phytoplankton biomass and therefore elevates chlorophyll level in the central North Pacific. Increase in the modeled chlorophyll expand the chlorophyll transitional zone and push the TZCF equatorward. Historical fishery catch data near the TZCF might yield some information to confirm the interdecadal migration patterns of the TZCF in the central North Pacific.

1. Introduction

The North Pacific Transition Zone (NPTZ) is bounded by two oceanographic fronts at approximately 30-32^{o}N (Subtropical Front) and 42-45^{o}N (Subarctic Front) in the central Pacific (Roden, 1991). The northern boundary of the subtropical gyre, the Subtropical Front, is defined as the surface outcropping of the 17^{o}C isotherm and 34.8 isohaline (Roden, 1991), and it can migrate a few degrees latitudinally on seasonal and interannual time scale (Lynn, 1986). The best marker of the Subarctic Front is the 33 isohaline in the salinity front with lower salinity water located in the subarctic region (Favorite et al., 1976). Using the data collected on board the commercial cargo carrier *M/V Skaugran* between January 1995 and January 2001, Wong et al. (2002) documented the seasonal and interannual changes in surface properties in the north of the Subarctic Front and discussed in detail about differences and similarities between the eastern and western subarctic regions.

The Transition Zone Chlorophyll Front (TZCF) is a biological front within the NPTZ that separates the low chlorophyll subtropical gyres and the high chlorophyll subarctic gyres in the Pacific Ocean. Operationally, the TZCF is defined as the location of 0.2 mg/m^{3} surface chlorophyll (Polovina et al., 2001). The TZCF migrates seasonally due to the extension or contraction of subtropical and subarctic gyres. Analyzing satellite maps of surface chlorophyll in the North Pacific, Polovina et al. (2001) documented the TZCF which is over 8000 km in longitude with a winter position around 30^{o}N and summer position around 40^{o}N. The position and dynamics of the TZCF varied substantially during the 1998 El Nino and the 1999 La Nina (Polovina et al., 2001).

With just a few years of high resolution basin-wide SeaWiFs surface chlorophyll coverage, it is apparently that the TZCF is a dynamic feature that strongly influences pelagic marine resources. The location of the TZCF appears to be related with juvenile albacore tuna migration patterns within the transition zone (Polovina et al., 2001) and it has potential implications for albacore fishery. The TZCF has also been revealed as an important foraging and migration pathway for loggerhead turtles (*Caretta caretta*) in the central North Pacific by tracking turtles using satellite telemetry and comparing their routes with the TZCF observed by satellite (Polovina et al., 2000).

The high quality remote sensing ocean color data, i.e., SeaWiFs and OCTS, are available only for the past several years (1997 to present). There is a big gap between the CZCS data set (1978-86) and the SeaWiFS, therefore, detecting the interdecadal migration of the TZCF using the remote sensing data is not possible at present. Sparse observations suggest that the position of the front varies on the interdecadal time scale but the limited chlorophyll measurements cannot provide a complete description of how the TZCF migrates in response to the Pacific Decadal Oscillation (PDO). Since the interdecadal climate variability significantly affects marine ecosystems in both subtropical and subarctic gyres (Karl et al., 2001; McGowen et al., 1998), it must consequently affect the positions of the TZCF.

Based upon the Hawaii Ocean Time-series (HOT) program and the limited historical data, Karl et al. (2001) reported that primary productivity in the subtropical gyre increased after 1976-77 regime shift. Analyzing and comparing apparent oxygen utilization (AOU) from four meridional transects through the northeast subtropical Pacific between 1980 and 1997, Emerson et al. (2001) found an increase in AOU by 20-25% over the past two decades and suggested an increase in oxygen demand by the biological pump and/or oxygen degassing by upper-ocean ventilation were accountable for the observed AOU increase.

Interdecadal physical variability in the subarctic Pacific has been observed in a number of ocean and atmospheric variables (Trenberth and Hurrell, 1994). The one of well-documented climatic changes in the North Pacific occurred during the period of 1976-77, when the intensification of the Aleutian Low pressure system resulted in a southward shift of the westerly winds, a stronger winter circulation at mid-latitudes, and enhanced surface ocean sensible and latent heat fluxes (Graham, 1994; Miller et al., 1994). Variations of oceanic physical variables have a series of implications on marine ecosystems (Mantua et al., 1997; Sugimoto and Tadoroko, 1997; McGowan et al., 1998). Widespread ecological changes associated with the 1976-77 climatic shift were observed throughout the North Pacific Ocean, ranging from plankton to the higher trophic levels (Venrick et al., 1987; Polovina et al., 1994; Francis and Hare, 1994). In the northwestern subtropical gyre region, chlorophyll in the spring showed a steady increase from the mid 1970s to the mid 1980s (Limsakul et al., 2001).

The dynamic linkages between ocean physics and biology on interdecadal scale are poorly understood because it is difficult to sample at the time and space scales necessary to elucidate the connections between large-scale physical processes and the smaller-scale biological responses (Miller and Schneider, 2000). In contrast, physical-biogeochemical models that express the interrelationships mathematically between physical forcing and the responses of ecosystem and biogeochemical processes can provide the necessary time and space scale resolution. Recently several basin scale ecosystem model studies, explicitly including the upper ocean biological processes, have been carried out. Chai *et al.* (1996 and 1999) incorporated an ecosystem model into a primitive equation circulation model to study nutrient cycles in the high nutrient and low chlorophyll (HNLC) environment for the equatorial Pacific. Kawamiya et al. (2000a and

b) embedded a six-component ecosystem into an ocean general circulation model (OGCM) of the North Pacific, and successfully reproduced spatial distribution and seasonal variations of biological variables. Haigh et al. (2001) embedded a simple biological model in an isopycnic general circulation model, and their physical-biological model reasonably reproduced the spatial patterns and seasonal changes in SeaWiFS images. Also, their modeled results showed deepening of the mixed layer depth in the subtropical gyres and shallowing in several regions of the subpolar gyres, which increased in the modeled nutrient concentration in the subtropical regions after 1976 correlated with increased plankton biomass.

Analyzing the estimated winter and spring mixed layer depth (MLD) from the National Oceanographic Data Center (NODC) temperature data, Polovina et al. (1995) found that winter and spring MLD in the subtropical and transition zone was 30-80% greater during 1977-88 than during 1960-76, while in the subarctic zone the MLD was 20-30% shallower. They also employed a simple plankton model forced with observed MLD and nutrients, and found that deepening in mixed layer might increase phytoplankton production in nutrient-poor subtropical regions by supplying more nutrients from depth, shallowing MLD in the subarctic would also increase production by increasing light availability to phytoplankton cells within the mixed layer. In between the subtropical and subarctic regions, both nutrient supply and light availability likely co-limit phytoplankton production, but how these processes change on the interdecadal time scale is not clear.

In order to improve our understanding of the dynamics that control the position of the TZCF and its interdecadal variability, we present a 30-year (1960-1990) retrospective analysis for the Pacific Ocean based upon the physical-biological model simulation. Our goal is to provide modeled evidence of interdecadal changes in the TZCF position and identify the responsible factors.

2. Model Description

2.1. Physical Circulation Model

The physical model is the oceanic component of the National Center for Atmospheric Research (NCAR) Climate System Model (CSM) (Gent et al., 1998), which is a modified version of the Geophysical Fluid Dynamic Laboratory (GFDL) Modular Ocean Model (MOM 1.1, Pacanowski et al., 1993). We have configured the model for the Pacific Ocean and the model performance has been reported in Li et al. (2001). The nonlocal KPP mixing scheme developed by Large et al. (1994) is incorporated into the model to better capture the small-scale physics within upper mixed layer and interior internal waves and double diffusion activities in the deep ocean. The Gent and McWilliam (1990) eddy-induced isopycnal mixing parameterization is applied. A third order upwind differencing scheme (Holland et al., 1998) is used to compute all tracers including temperature, salinity and biochemical components. The horizontal and vertical background mixing coefficients tracers (temperature, salinity, and all biological components) are chosen to be 2×10^6 cm^2/sec and 0.1 cm^2/sec, respectively. The latter turns out to be critical to maintain realistic vertical patterns of tracers within thermocline. The vertical viscosity (for velocity calculation) is chosen to be 1.0 cm^2/sec, an order larger than background mixing, while the horizontal viscosity is 5×10^6 cm^2/sec.

The Pacific Ocean model domain is between 45°S and 65°N, 100°E and 70°W, with realistic geometry and topography. The longitudinal resolution of the equatorial Pacific is 2° everywhere, while the latitudinal is 0.5° within 10°S and 10°N, tapering off to 2° at high latitude. There are 40 vertical layers, with 23 levels located in the upper 400m. The boundaries at 45^{o}S and 65^{o}N are closed walls and no flow is allowed through the boundary. In the regions near the two closed walls, a sponge layer of 10^{o} wide from the walls is applied. A decay term □(T*-T) is added to the tracer equations with T representing temperature, salinity, nitrate and silicate. T* represents the observed temperature, salinity, nitrate and silicate fields taken from NODC World Ocean Atlas (Levitus et al., 1994). The □ value vary smoothly from 50 day^{-1} at the north or south walls to zero at 10 degrees away from the walls.

2.2. Biological Model

The biological model is developed originally for the equatorial Pacific Ocean to study the nitrogen and silicon cycles in the equatorial Pacific (Chai et al., 2002; Dugdale et al., 2002; Jiang et al., accepted). The 1-D model has been tested against the JGOFS data over the equatorial Pacific and is capable of reproducing the Low-Silicate, High-Nitrate, Low-Chlorophyll (LSHNLC) conditions in the equatorial Pacific. The biological model (Figure 1) consists of ten compartments describing two size classes of phytoplankton (P1, P2) and zooplankton (Z1, Z2), detrital nitrogen (DN) and detrital silicon (DSi), silicate ($Si(OH)_4$), and total CO_2 and two forms of dissolved inorganic nitrogen: nitrate (NO_3) and ammonium (NH_4), which are treated separately, thus enabling division of primary production into new production and regenerated production. P1 represents small, easily grazed phytoplankton whose specific growth varies, but whose biomass is regulated by micrograzers (Z1) and whose daily net productivity is largely remineralized (Landry et al., 1997). P2 represents relatively large phytoplankton (> 10 µm) that makes up high biomass blooms and contributes disproportionately to sinking flux as ungrazed production or large fecal pellets (Wefer, 1989; Bidigare and Ondrusek, 1996). The P2 class represents the diatom functional group, and has the potential to grow fast under optimal nutrient conditions (Coale et al., 1996). Z1 represents small micrograzers whose specific growth rate are similar to P1 phytoplankton whose grazing rate is density dependent (Landry et al., 1997) and Z2 the larger mesozooplankton that graze on P2 and detrital nitrogen (DN) and prey on Z1. The Z2 zooplankton have a feeding threshold with conventional grazing dynamics as described in Frost and Franzen (1992).

Below the euphotic zone, sinking particulate organic matter is converted to inorganic nutrients by a regeneration process similar to the one used by Chai et al. (1996), in which organic matter decays to ammonium, and then is nitrified to NO_3. The flux of particulate material is specified using an empirical function from Martin et al. (1987). The silicate regeneration is modeled through a similar approach but with a deeper regeneration depth profile, which reflects biogenic silica tends to have higher preservation efficiency compared to other particulate organic matter (Ragueneau et al., 2000). The detailed equations and parameters used for the biological model were presented in the paper by Chai et al. (2002).

2.3. Initial Conditions and Surface Forcing

The physical model is initialized with NODC World Ocean Atlas climatological January temperature and salinity (Levitus and Boyer, 1994; Levitus et al., 1994) with zero velocities. The nutrients (nitrate and silicate) are initialized with NODC World Ocean Atlas climatological annual mean values (Levitus et al., 1993). For other components in the biological model, they are assigned with 0.25 mmol m^{-3} at the surface, decreasing exponentially with a scale length of 120 m, which is the depth of euphotic zone. Chai (1995) showed that the initial conditions in the euphotic zone for the biological model did not alter the final results because the biological model reached the equilibrium faster than the physics did.

The surface forcing can be separated into momentum, heat, fresh-water fluxes, and light for the photosynthesis. The momentum fluxes are calculated with the zonal and meridional wind speeds from the Comprehensive Ocean Atmosphere Data Set (COADS) (da Silva et al., 1994). COADS is selected because it is the longest surface marine dataset covering the entire Pacific Ocean. The heat flux calculation includes short wave radiation, outgoing long wave radiation, and both sensible heat and latent heat fluxes. The surface salinity is restored to the NODC climatological monthly mean salinity (Levitus et al., 1993). More details about surface physical forcing treatment can be found in Li et al. (2001). The surface light intensity (I_o) is converted from the monthly mean COADS short wave radiation (R_s) using $I_o = 0.5*R_s$. Since the monthly averaged short wave radiation is used, the day-night cycle of light is not resolved in the current model, rather the daily averaged light is used for photosynthesis calculation.

The ecosystem governing equations are solved simultaneously with the physical model. The physical-biological model is integrated for 10 years from the initial conditions. During this 10-year period, the model achieves a quasi-equilibrium state of annual cycle in the upper ocean. Then monthly mean forcing from January 1955 to December 1993 is used to force the coupled physical-biological model. This paper focuses on the model results from period between January 1960 and December 1990.

3. Results and Discussion

3.1. Modeled Seasonal Migration of the TZCF

Based upon the same circulation model configurations, the model performance of the physical conditions and its variability have been reported by Li et al. (2001). By compared two different vertical-mixing schemes, Pacanowski and Philander (PP) and K-Profile Parameterization (KPP), Li et al. (2001) found that KPP is significantly better than the PP scheme in simulating the thermal and current structures, including the annual mean, annual cycle, and interannual-to-interdecadal variability. Li et al. (2001) also documented comparisons in detail between the modeled physical properties with the observations. In this paper, we focus on the modeled ecosystem response to physical variability in the central North Pacific.

The Pacific Ocean, by far, is the largest ocean in the world. The immense size of the Pacific is reflected in strong spatial differences in mixed layer depth, thermocline depth, upwelling velocity, and other physical features, which results in diverse regional oceanic ecosystems (Longhurst, 1998). The biological processes respond to variations in physical forcing functions such as solar radiation and surface wind on a variety of timescales, spring bloom of phytoplankton biomass is the dominant temporal feature in the western subarctic gyres, and it is essential for biological models to capture spring blooms both in spatial pattern and intensity (Frost and Kishi, 1999). The modeled spring (April-May-June) surface chlorophyll, converted from the modeled phytoplankton biomass, compares well with the historical *in situ* chlorophyll measurements in the western and central subarctic regions (NODC World Ocean Atlas 1998, Conkright et al., 1998), Figure 2.

On the other hand, in the northeast subarctic region, the model tends to produce surface chlorophyll level higher than the observational data. The Ocean Station Papa (OSP) at 50^{o}N and 145^{o}W in the subarctic Northeast Pacific, surface chlorophyll only increases slightly during late spring and early summer, from 0.2 to 0.4 mg/m^3 (Harrison, 2002), whereas the modeled spring and early summer surface chlorophyll level is around 0.6 to 0.8 mg/m^3, about a factor of 2 higher than the observations. This is mainly due to inadequate treatments of iron limitation for the subarctic Northeast Pacific with the present ecosystem model structure. The OSP has been characterized as a high nitrate and low chlorophyll (HNLC) region where iron limits the growth of large diatoms in late spring and summer (Martin and Fitzwater, 1988), iron and irradiance co-limit in the winter (Maldonado et al., 1999). The current ecosystem model considered the role of iron for the equatorial Pacific Ocean, also a HNLC region, with incorporating the effects of iron limitation implicitly through the parameters that determine the growth rate of diatoms (Chai et al., 2002). Several iron enrichment experiments were conducted by changing the parameter $\square$ (the initial slope of the photosynthetic rate over irradiance at low irradiance) and $\square 2_{max}$ (the potential maximum specific diatom growth rate) in the regulation terms of silicate uptake by diatom (Chai et al., 2002). The values for these parameters were selected based upon the observations for the equatorial Pacific Ocean (Barber and Chavez, 1991; Barber et al., 1996), which may not be suitable for the OSP in subarctic Northeast Pacific. Denman and Pena (1999) developed an ecosystem model for the OSP and addressed the iron limitation implicitly with the similar approach used by Chai et al. (1996 and 1999) for the equatorial Pacific. Due to the drastic differences between the model structures, it is unlikely at present that we can incorporate iron limitation properly for both the equatorial Pacific and the subarctic Northeast Pacific at the same time. In summary, our present ecosystem model has a weaker iron limitation for the OSP, therefore, it produces stronger spring to summer chlorophyll transition, and the phytoplankton seasonal cycle is determined mainly with the light limitation and the depth of the mixed layer. In the future, ecosystem model development needs to consider the iron limitation explicitly which can produce multiple HNLC regions simultaneously.

Due to lack of horizontal resolution (2^o in longitude) near the coastal regions, the model does not resolve chlorophyll conditions associated with the coastal upwelling, such as along the coast of California. The domain of this physical-biological model was designed to study oceanic biological processes on the basin-scale and, therefore, it is not suitable for investigating coastal processes.

In the subtropical gyre (south of 28^oN), both the modeled and in situ chlorophyll tend to be much lower than the subarctic region, around 0.1 mg/m^3 or less. A biological front, normally located between 28^oN and 40^oN, that separates the low chlorophyll subtropical gyres and the high chlorophyll subarctic gyres in the Pacific Ocean, is refereed to as the Transition Zone Chlorophyll Front (TZCF) (Polovina et al., 2001). Analyzing remote sensing images of surface chlorophyll, Polovina et al. (2001) found that a chlorophyll concentration of 0.2 mg/m^3 is a good indicator of the TZCF positions. The isopleth of 0.2 mg/m^3 chlorophyll migrates seasonally due to the extension or contraction of subtropical and subarctic gyres. For example, during the winter season (January to March), a 0.2 mg/m^3 chlorophyll front is located between 26^oN and 27^oN in the central Pacific, and it is located between 34^oN and 35^oN during the summer season, as shown in Figure 3. During the winter and early spring, stronger vertical mixing enhances supply of nutrients and photosynthetic available radiation (PAR) is relatively adequate in the TZCF, especially in the southern section. These conditions are favorable for enhancing phytoplankton growth, which results in pushing the 0.2 mg/m^3 chlorophyll front equatorward to between 26°N and 27°N. On the other hand, increase in surface heat flux into the ocean results in stronger stratification during the summer (July to September), which reduces vertical nutrient flux. Therefore, the primary productivity is reduced as spring progresses to summer, and the 0.2 mg/m^3 chlorophyll front moves poleward to between 34°N and 35°N.

Analyzing the OCTS and SeaWiFS data between January 1997 and December 1999, Polovina et al. (2001) have found there was considerable interannual variation in the positions of the TZCF, with the largest seasonal shift of 1000 km during 1998, but a much smaller seasonal migration of the TZCF during 1999 (their Figure 9). The modeled 0.2 mg/m^3 chlorophyll fronts (Figure 3) exhibit about 700-1000 km seasonal shift in the western and central North Pacific. In the eastern part of the basin, the seasonal migration of the TZCF is less pronounced which is similar to the pattern reported by Polovina et al. (2001). Overall, the modeled seasonal migrations of the TZCF, about 700-1000 km in the western and central Pacific, are comparable with the satellite observations. But, the modeled TZCF positions tend to be located more in the southern latitudes compared to the satellite observations during both seasons. This could be due to the general offset between the modeled surface chlorophyll and the satellite observations. In the model, a constant factor for the entire Pacific basin is used to convert the modeled surface phytoplankton biomass (mmol N/m^3) to chlorophyll (mg/m^3). This conversion factor could vary spatially as well as seasonally, but lack of the information prevents us to assign this conversion factor as a variable for the present ecosystem model. It has to be pointed out that the modeled TZCF represents long term climatological mean conditions, whereas the satellite derived TZCF positions (Polovina et al., 2001) are only for the period of 1997-99. There have been some indications that a flip from warm to cool PDO phases may have taken place in 1998 (Mantua and Hare, 2002), which could result in shifting overall positions of the TZCF after 1998.

3.2. Modeled Interdecadal Variability of the Mixed Layer Depth and Ekman Pumping

The variability of the TZCF on the interdecadal timescale likely can be viewed as the manifestation of biological response of both subtropical and subarctic gyres to climate variability. Using a coupled physical-biological model forced with the observed surface wind stress and heat flux, the movement of the TZCF in response to the interdecadal forcing has been resolved, but the modeled physical changes are described first.

The mixed layer depth (MLD) during winter regulates supply of nutrients into the euphotic zone, and consequently a potential increase in the spring phytoplankton transition in the western and central subarctic regions. The MLD is controlled mainly by the strength and spatial pattern of the surface wind stress, therefore, changes in the wind stress are reflected in the modeled MLD. In the model, the MLD is defined as the depth where potential density (σ_t) is 0.125 kg/m^3 higher than its surface value at each grid point. The winter time (January-March) MLD is averaged over two periods, 1979-90 and 1964-75, in order to detect the modeled interdecadal changes, Figures 4 (a) and 4 (b). The model reproduces the winter MLD patterns similar to the observations (Monterey and Levitus, 1997) and other circulation modeling results (Kawamiya et al., 2000a, their Figure 5a). In general, the maximum MLD is located in the Kuroshio-Oyashio extension region in the northwestern Pacific, with values exceeding 200 m. For the central and northeastern Pacific, the winter MLD ranges between 50 to 100 m. Despite the coarse resolution of the circulation model, 1^{o} X 2^{o} in the mid and high latitude, the simulated

MLD seems reasonable. One of the model improvements is incorporation of the nonlocal KPP mixing scheme, which does a better job in capturing the small-scale physics within the upper mixed layer and interior internal waves (Large et al., 1994; Li et al., 2001). Because of the improvements of mixed layer dynamics, the coarse resolution circulation model seems to be able to capture the upper thermal structure changes on interannual-to-interdecadal time scale as well. For the Kuroshio Current Extension region (34^o-42^oN, 140^oE-180^o), Li et al. (2001) compared the modeled monthly temperature anomalies with the observations by Deser et al. (1996), and found similar trend and magnitude of changes of temperature in the top 400 m from 1970 to 1991 (their Figure 14).

A major climatic regime shift occurred in the mid-1970s. The Aleutian Low pressure system intensified and subtropical westerly winds strengthened (Trenberth and Hurrell, 1994), which cause the winter and spring MLD to increase by 30-80% in the subtropical gyre and the transition zone (Polovina et al., 1995). The modeled winter MLD difference between 1979-90 and 1964-75 shows the largest increase which is located between 30^oN and 40^oN in the central Pacific (150^oE to 180^o), with a value of 40-60% higher (deeper mixed layer) during 1979-90 relative to 1964-75 values, Figure 4 (c). In the subarctic gyre (north of 40^oN) in both northeastern Pacific (Ocean Station Papa) and Oyashio region (northwestern Pacific), the modeled MLD decreases by about 20% during the period of 1979-90 relative to 1964-75 levels. Several studies based upon the historical hydrographic data have detected a gradual decrease of the winter MLD during the past several decades both in the eastern (Freeland et al., 1997) and western (Ding and Saino, 1999) subarctic North Pacific. The modeled winter MLD changes in the northeastern (Ocean Station Papa) and northwestern (Oyashio region) Pacific, agree with the observed declining trend of the winter MLD.

The modeled winter MLD difference closely resembles the spatial patterns and the magnitude of change of findings based upon the NODC temperature profile data by Polovina et al. (1995), their Figure 3. The model is designed to capture the basin-scale and long term variability, and the coastal dynamics might not be well resolved. For example in the Gulf of Alaska, where the modeled MLD difference between 1979-90 and 1964-75 is relatively small, the NODC data indicates about 20-30% shallower in the winter and spring MLD during the period of 1977-88 (Polovina et al., 1995). Unlike the treatment of the surface heat flux calculation, the present model is always forced with the monthly averaged climatological salinity values, hence there is no interdecadal signal in the modeled surface salinity field. Haigh et al. (2001) analyzed the NODC salinity data for two different periods, 1952-75 and 1977-88, and found that an overall fresher of the surface water in the subarctic region and the Gulf of Alaska after 1976-77, which could contribute even more shallowing of the MLD in these regions. The role of surface salinity changes on interdecadal time scale should be considered in the future circulation model simulations.

In spite of the coarse resolution of the present circulation model and lack of surface salinity variability on the interdecadal timescale, overall, the model produces winter MLD changes before and after the 1976-77 climatic shift that are very similar to the NODC observational data (Polovina et al., 1995; Deser et al., 1996) as well as other circulation model results (Miller and Schneider, 2000; Xie et al., 2000).

Although the circulation model with the KPP scheme has made significant improvement in simulating the interdecadal variability in the mixed layer dynamics as well as the upper ocean thermal structures, there is sill room for improvement. Overall circulation model can be improved by increasing horizontal resolution in order to resolve some local dynamics, such as the Kuroshio-Oyashio transition zone. The present coarse resolution circulation model is insufficient to reproduce the Kuroshio detachment adequately (Kobayashi, 1999), and this issue could be important for the formation of water masses spreading into the entire subtropical gyre. So, resolving the Kuroshio-Oyashio transition zone dynamics is relevant not only to the mixed layer dynamics in the local region alone, but also to other regions as well. Another improvement of future circulation modeling is the sensitivity of the KPP scheme to salinity and freshwater flux and its potential impact on simulating the interdecadal thermal variability, which requires a better evaporation and precipitation fields at ocean surface.

The wind stress curl (the spatial pattern in the surface wind stress) determines the Ekman pumping velocity which forces the thermocline directly. The Ekman pumping velocity (upward positive) is defined as:

$$W_e = \mathrm{curl}(\tau/f)/\rho = [\mathrm{curl}(\tau) + \beta_x \tau/f]/(f\rho) \qquad (1)$$

Here τ is the wind stress, τ_x its zonal component, ρ water density, and β is the latitudinal derivative of the Coriolis parameter. Variability in the Ekman pumping velocity, a reflection of both the wind stress curl and the zonal wind stress, not only impacts on the thermocline variation but also influences the depth of the nutricline, furthermore, phytoplankton productivity. Examining decadal variability of the Ekman pumping velocity elucidates the winter nutrient concentration changes in the upper ocean which determines intensity of the spring phytoplankton bloom. The annual mean Ekman velocity follows the winter time (January-March) Ekman velocity very closely, but its intensity is reduced compared to the winter time value. Therefore, the winter time Ekman pumping velocity is presented for the discussion.

The winter (January-March) Ekman pumping velocity is averaged over two periods, 1979-90 and 1964-75, Figures 5 (a) and 5 (b). The positive Ekman pumping dominates the subarctic gyre with two maxima centered in both western and eastern regions. In the transition zone, between 30^{o}N and 45^{o}N, the winter Ekman pumping velocity overall is positive except in a smaller region in the eastern part of the basin away from the coast. The upward Ekman pumping in the transition zone brings nutrients to the euphotic zone that sustains phytoplankton production in the transition zone and pushes the surface chlorophyll front equatorward during the winter (Figure 3). In the subtropical gyres, south of 30^{o}N, the Ekman pumping velocity is negative (downward). The overall downward motion in the thermocline depth causes a lack of nutrient supply and limits phytoplankton production in the subtropical gyres (Figure 2). There is a zonal difference in the Ekman pumping velocity in the subtropical gyres with more intensified downward motion in the west and less so in the east. The winter Ekman pumping velocity field in the subtropical gyres is consistent with the calculation based upon the historical hydrographical data by Suga et al. (2000, their Figure 16).

The difference in the winter Ekman pumping velocity between 1979-90 and 1964-75 shows the largest increase located between 30^{o}N and 45^{o}N in the central and eastern Pacific (180^o to 150^{o}W), Figure 5 (c). The maximum increase of the winter Ekman pumping velocity centered along 35^{o}N is more than doubled during 1979-90 relative to the 1964-75 values. Comparing to the largest difference of the modeled winter MLD (150^{o}E to 180^o, Figure 4c), the maximum increase of the winter Ekman pumping velocity locates further to the east (170^{o}E to 150^{o}W), and both are found in the latitudinal band between 30^{o}N and 45^{o}N, i.e., the transition zone. In the subarctic northeastern region including the Gulf of Alaska, the winter Ekman pumping velocity decreases by about

25% during the period of 1979-90 relative to 1964-75 levels. In the region south of 30°N, the downward Ekman pumping strengthens during the period of 1979-90, which produces the negative anomalies in the most areas of that region (Figure 5c). The spatial pattern of the winter Ekman pumping velocity difference is complex in the North Pacific, and it is caused by the surface wind stress changes during different decades. Analyzing the NCEP reanalysis wind stress from 1958 to 1997, Xie et al. (2000) found the similar spatial pattern and its interdecadal variations for the Ekman pumping velocity, their Figures 11 and 12. This provides the evidence that the COADS wind stress and wind stress curl are not unique or biased in terms of the interdecadal variability.

Both NCEP reanalysis and COADS wind stress result in very similar Ekman pumping velocity and associated interdecadal variations, but causes for the wind stress changes on interdecadal timescale are still unclear. Miller et al. (in press) discussed and summarized several mechanisms responsible for interdecadal climate variations over the Pacific Ocean including the potential influence of the oceanic biological processes that might have a significant feedback to the physical climate system. In this paper, we focus on the direct biological response to the interdecadal physical forcing, the potential feedback from the oceanic ecosystem to the physical processes is not included in this modeling study.

3.3. Modeled Interdecadal Variability of the Nutrient and Primary Productivity

The positive upward Ekman pumping and deeper MLD during the winter in the western and central subarctic gyres and the transition zone elevate surface nutrient concentration, which set up necessary conditions for enhanced phytoplankton productivity in the spring. The winter (January-March) modeled surface nitrate concentration is averaged over two periods, 1979-90 and 1964-75, Figures 6 (a) and 6 (b). The highest winter surface nitrate concentration is in the northwestern Pacific between 45°N-55°N and 150°E-180°, with the surface values exceed 20 mmol/m^3. In the northeastern Pacific, for example near the Ocean Station Papa (OSP) (50°N and 145°W), the modeled winter nitrate concentration is about 15 mmol/m^3 which agrees with the OSP winter nitrate value of 15.8 mmol/m^3 (Harrison, 2002, his Table 1). In addition to the strong north-south gradient, the east-west contrast of the modeled surface nitrate in the subarctic gyre (north of 40°N) is also pronounced. Overall, the model produces the winter surface nitrate distribution and concentration comparable to the NODC WOA98 (Conkright, et al., 1998), and especially agrees with the surface nitrate observations collected through the Canada-Japan ship-of-opportunity program between January 1996 and January 2001 (Wong et al., 2002, their Figure 3d). The modeled surface nitrate concentration also compares well with other physical-biological modeling studies for the North Pacific (Kawamiya et al., 2000a, their Figure 7; and Haigh et al, 2001, their Figure 2).

The modest interdecadal physical variability affects the nutrient supply to the euphotic zone which, in turn, affects phytoplankton productivity and, eventually, higher trophic levels (Venrick et al., 1987; McGowen et al., 1998). The modeled winter surface nitrate difference between 1979-90 and 1964-75 shows increase in the latitudinal band of 30°N and 45°N from the west to the east (135°E-135°W), with two maxima (about 4 mmol/m^3) located in the north of Japan (45°N and 140°E) and central northeastern Pacific (40°N and 150°W). The modeled nitrate concentration is about 10 to 50% higher in general during the period of 1979-90 relative to 1964-75 values depending upon locations. The increase is found mainly along the 10 mmol/m^3 isopleth of nitrate concentration during the 1964-75 period, which indicates the 10 mmol/m^3 isopleth of the modeled nitrate moves equatorward during 1979-90. From the perspective of nitrate increase after 1976-77, the subarctic gyre expanded which resulted in an increase of surface nitrate concentration in the transitional zone (30^{o}N to 45^{o}N) during 1979-90. The winter surface nitrate concentration difference (Figure 6c) is caused by a combination of the winter MLD difference (Figure 4c) and winter Ekman pumping velocity difference (Figure 5c), and seems to follow the latter more closely.

The spatial distribution of the modeled surface nitrate concentration difference is consistent with several direct and indirect observations. For example, in the central North Pacific, Venrick et al. (1987) found that the averaged euphotic zone (0-200 m) chlorophyll concentration in the oligotrophic region during summer (May-October) had nearly doubled from 1968 to 1985. Their data collected from the Climax region (26.5-31.0^{o}N and 150.5-158.0^{o}W) also indicated decrease in sea surface temperature, which suggests increase in surface nutrients. The area of the largest increase in the modeled winter surface nitrate is between 30^{o}N and 45^{o}N, and it varies longitudinally. The very southern edge of the modeled surface nitrate changes overlaps with the northern edge of the Climax region (31^{o}N). Since the modeled surface nitrate focuses on the winter season (January-March), and insufficient sampled Climax data was mainly for the summer season (May-October), it is difficult to make direct and detailed comparison between the modeled results and the Climax observations. Combining the data collected from the ongoing Hawaii Ocean Time series (HOT) program and the Climax data for the North Pacific Subtropical Gyre, Karl et al. (2002) have also documented that mean euphotic zone chlorophyll concentration from the period October 1988 to December 1997 is also significantly greater than the averaged pre-1976 Climax program chlorophyll concentration (their Figure 9.12). Unfortunately, our model simulation ends on December, 1993, due to the lack of processed COADS surface observations after 1993. The direct comparison with the HOT observations could not be done with our current model simulations. It seems that the largest decadal variations occurred in the north of HOT and Climax regions according to the modeled results, but there were no any other direct and consistent observational data in these areas to confirm such findings at present.

Analyzing and comparing oxygen utilization (AOU) from four meridional transects along 152^{o}W (or 155^{o}W) between 45^{o}N and Hawaii during the past two decades, Emerson et al. (2001) found an increase of AOU by 20-25% and it could result from an increase in biological productivity. Ono et al. (2001) analyzed the hydrographic observations (only winter data was selected) from 1968 to 1998 in the Oyashio region (39^{o}N to 43^{o}N, 143^{o}E to 149^{o}E) and found that there was a linear increasing trend in both phosphate and AOU in subsurface (deeper than 100m), for which agrees with our modeled nitrate difference (not shown for the subsurface difference). Moreover, Ono et al. (2001) suggested the linear increasing trend in subsurface phosphate and AOU may not be caused by the bidecadal oscillation (20 years) but correspondent to the longer-term process such as pentadecdal (50 years, e.g., Minobe, 1999) or anthropogenic effects. On the other hand, Ding and Saino (1999) found that the winter MLD in the same location (the Oyashio region) decreased since 1968, which our modeled winter MLD shows the similar trend (Figure 4c). Ding and Saino (1999) also found that nutrient concentration in the mixed layer decreased whereas our modeled result shows an increase in the surface nitrate in that region (Figure 6c). The modeled surface nitrate increases due to the positive anomaly of the winter Ekman pumping velocity between 1979-90 and 1964-75, (see Figure 5c). Even though the winter MLD shallowed in the Oyashio region after

1976-77, the enhanced winter Ekman pumping in this region pushes the subsurface nitricline upward which results in the increase in the subsurface nitrate, and potentially surface nitrate as well. More detailed model and data comparison is needed for the regions where historical hydrographic data exist, especially for any long term changes in the vertical structure.

In the northeastern Pacific, for example the Ocean Station Papa (OSP, 50^oN and 145^oW), Freeland et al. (1997) found that the observed winter nitrate concentration within the upper 100 m decreased since 1970 with a declining trend of about 16.3 $mmol/m^3$/century, their Figure 7. The modeled winter surface nitrate concentration at the OSP changed about 2 $mmol/m^3$ between 1979-90 and 1964-75 (Figure 6c), which agrees well with the observed declining rate. The shallowing in the winter MLD at the OSP, due to the combination of warming and freshening at sea surface, caused overall reduction in nitrate concentration in the upper ocean (Freeland et al., 1997). In the model, the winter surface nitrate decreasing trend at the OSP is caused by the combination of the winter MLD decrease (Figure 4c) and negative anomaly of the winter Ekman pumping (Figure 5c) which reduces the upward Ekman motion after 1976-77. Further examining of the changes in the vertical nutrient profiles at the OSP may yield more information about the interdecadal variability of upward nutrient flux, therefore productivity and biomass changes at the OSP.

The spatial pattern of the modeled winter nitrate difference between 1979-90 and 1964-75 is complex; it is mainly associated with the large scale wind pattern changes both in wind stress intensity and wind stress curl. The change in the surface nitrate concentration certainly has an impact on phytoplankton productivity and surface chlorophyll distribution. Since the interdecadal variation of the TZCF is one of the focuses of this paper, we concentrate analysis on the modeled productivity changes in the NPTZ.

In the central North Pacific, 30°N-40°N and 180°-140°W, the modeled vertically integrated (0-100 m) primary production anomaly was obtained by removing the seasonal cycle and then a 7-year running mean was applied to the anomaly field in order to remove the interannual variability, Figure 7a. Overall, the modeled primary production anomaly tracks the Pacific Decadal Oscillation (PDO) index very closely, with lower productivity during the negative PDO phase before 1976-77 and higher production values after. In the above defined region, the area averaged mean seasonal cycle of the integrated (0-100m) primary production ranges from 10.1 mmol C/m^2/day in the winter to 40.5 mmol C/m^2/day in the spring, with the annual mean value of 29.8 mmol C/m^2/day. The amplitude of modeled primary production anomaly is 6.3 mmol C/m^2/day with the highest value of 3.6 mmol C/m^2/day during early 1980s and the lowest value of -2.7 mmol C/m^2/day during mid 1960s. Before and after 1976-77 climate shift, the modeled primary productivity increased by about 21% relative to the annual mean values (6.3/29.8=0.21).

The modeled primary productivity increase is caused by the enhanced surface nitrate in the central North Pacific (Figure 6c). The sharp increase in the modeled primary productivity occurs around 1976-77 when the PDO index switches from negative to positive, which causes an increase of the winter MLD and strengthened Ekman pumping. This indicates that the lower trophic primary producers in the marine ecosystem respond to the physical climate changes quickly, and the productivity tends to stay in one mode for a couple of decades or so before switching to the opposite phase. Such sudden switches in primary productivity seem to play an important role in determining which small pelagic fish dominate, as in the anchovy and sardine alternation at similar periods of around 20 years (Chavez et al., 2003).

Enhanced primary productivity after the 1976-77 climatic shift contributes higher phytoplankton biomass and therefore elevates chlorophyll level in the central North Pacific. Increase in the modeled chlorophyll expands high chlorophyll area in the NPTZ and pushes the TZCF equatorward. In order to detect the TZCF position changes, the anomaly field of the 0.2 mg/m^3 surface chlorophyll monthly position (it includes all seasons, not just winter time) was obtained by removing its seasonal cycle and a long term running mean filter was applied, Figure 7b. As a reference for the interdecadal changes, the anomaly field of the Ekman pumping velocity averaged over the region (30^{o}N-40^{o}N and 180^{o}-140^{o}W) was also plotted in Figure 7b. Prior to the 1976-77, the 0.2 mg/m^3 surface chlorophyll front is located 1^{o} northward (positive anomaly) from the long term mean positions (0^{o} line). After the 1976-77, the 0.2 mg/m^3 surface chlorophyll front moves southward about 1.5^{o} (negative anomaly) during 1980s . The amplitude of north-south migration of the 0.2 mg/m^3 surface chlorophyll front is about 2.5^{o} (about 250 km) between 1964-75 and 1979-90. After the 1976-77 climatic shift, the higher chlorophyll area in the NPTZ expanded and the TZCF migrated equatorward from the long term mean position.

The location of the TZCF appears to be related with juvenile albacore tuna migration patterns within the transition zone and it has potential implications for albacore fishery. Polovina et al. (2001) found that the 3-5-year-old albacore being caught by the troll fishing fleet are exploiting the TZCF as migration route and as forage habitat during their trans-Pacific migration. Furthermore, they have found that both albacore fishing effort and the highest albacore catch-per-unit of effort (CPUE) are concentrated along the

TZCF (their Figure 5, Polovina et al., 2001). The interdecadal movement of the TZCF is important especially its relationship to the fishery, but it is very difficult to be confirmed directly with surface chlorophyll measurements. The high quality remote sensing ocean color data, i.e., SeaWiFs and OCTS, are available only for the past several years (1997 to present). There is a big gap between the CZCS data set (1978-86) and the SeaWiFS, therefore, detecting the interdecadal migration of the TZCF using the remote sensing data is not possible at present. Historical fishery catch data near the TZCF might yield some information on how the TZCF migrated during the past several decades, which may provide a test for the physical-biological modeled results regarding the interdecadal movement of the TZCF. Such a study is needed in order to improve physical-biological model performance and reliability, furthermore, to accurately assess climatic and human influences on the marine ecosystem.

Conclusions

A three-dimensional physical-biological model has been used to study interdecadal variation of the transition zone chlorophyll front (TZCF) in the central North Pacific Ocean. The physical model is a modified version of Modular Ocean Model (MOM 1.1, Pacanowski et al., 1993), and configured for the Pacific Ocean by Li et al. (2001). The biological model is developed originally for the equatorial Pacific Ocean to study the nitrogen and silicon cycles by Chai et al. (2002) and Dugdale et al. (2002). The physical-biological model is forced with the monthly mean heat flux and surface wind stress from the Comprehensive Ocean Atmosphere Data Set (COADS) (da Silva et al., 1994). The physical-biological model results from the 30-year (1960-1990) retrospective analysis are as following:

1) The modeled spring surface chlorophyll reproduces the *in situ* chlorophyll observations in the western and central subartic regions, including the position of the TZCF, defined as the isopleth of 0.2 mg/m^3 surface chlorophyll. The modeled TZCF is located between 26^{o}N and 27^{o}N in the central North Pacific during winter and between 34^{o}N and 35^{o}N during the summer, which tends to agree with the satellite observed seasonal migration patterns of the TZCF (Polovina et al., 2001).

2) The interdecadal variability of modeled winter MLD shows the largest increase which is located between 30^{o}N and 40^{o}N in the central North Pacific (150^{o}E to 180^o), with a value of 40-60% higher (deeper mixed layer) during 1979-90 relative to 1964-75 values. In the subarctic gyre in both northeast (Ocean Station Papa) and northwest Pacific (Oyashio region), the modeled winter MLD decreases by about 20% during the period of 1979-90 relative to 1964-75 levels. Overall, the model produces the winter MLD changes

before and after the 1976-77 climatic shift, which are very similar to the historical observational data (Polovina et al., 1995; and Deser et al., 1996).

3) The interdecadal variability of the winter Ekman pumping velocity difference between 1979-90 and 1964-75 shows the largest increase which is located between 30^{o}N and 45^{o}N in the central and eastern North Pacific (180^{o} to 150^{o}W). In the subarctic northeast Pacific region including the Gulf of Alaska, the winter Ekman pumping velocity decreases during the period of 1979-90, but its value increases in the northwest Pacific (Oyashio region) after 1976-77 climatic shift. The Ekman pumping velocity difference before and after 1976-77 derived from the COADS surface wind stress agree with the results based upon the NCEP reanalysis by Xie et al. (2000).

4) The physical-biological model produces the winter surface nitrate concentration comparable to the observed values (Conkright, et al., 1998; Wong et al., 2002). The modeled winter surface nitrate difference between 1979-90 and 1964-75 shows an increase in the latitudinal band between 30^{o}N and 45^{o}N from the west to the east (135^{o}E-135^{o}W), the modeled nitrate concentration is about 10 to 50% higher in 1979-90 relative to 1964-75. The increase of the winter surface nitrate concentration during 1979-90 is caused by a combination of the winter MLD increase and the winter Ekman pumping enhancement after the 1976-77 climatic shift.

5) The modeled nitrate concentration increase after the 1976-77 climate shift results in increasing primary productivity in the central North Pacific (30^{o}N-40^{o}N and 180^{o}-140^{o}W). Enhanced primary productivity after the 1976-77 climatic shift contributes higher phytoplankton biomass and therefore elevates chlorophyll level in the central North Pacific. Increased chlorophyll expands the high chlorophyll area and pushes the

TZCF equatorward. The amplitude of north-south migration of the 0.2 mg/m^3 surface chlorophyll front is about 250 km between 1964-75 and 1979-90.

Acknowledgments: This research was supported by NASA and NSF Grants to F. Chai. Two anonymous reviewers provided comments that greatly improved the final version of the manuscript. F. Chai thanks Drs. T. Saino and K. Suzuki for the discussions during his sabbatical at the Nagoya University.

References

Barber, R.T. and F.P. Chavez (1991) Regulations of primary productivity rate in the equatorial Pacific, Limnology and Oceanography 36 (8), 1803-1815.

Barber, R.T., S.T. Lindley, M. Sanderson, F. Chai, J. Newton, C.C. Trees, D.G. Foley, and F. Chavez (1996): Primary production in the equatorial Pacific during 1992. *Deep-Sea Res. II,* Vol. **42**, No. 4-6, 933-969.

Bidigare, R. R. and M. E. Ondrusek (1996): Spatial and temporal variability of phytoplankton pigment distributions in the central equatorial Pacific Ocean. *Deep-Sea Research* II 43: 809-833.

Chai, F., R. C. Dugdale, T-H Peng, F. P. Wilkerson, and R. T. Barber (2002): One Dimensional Ecosystem Model of the Equatorial Pacific Upwelling System, Part I: Model Development and Silicon and Nitrogen Cycle. *Deep-Sea Res. II*, Vol. 49, No. 13-14, 2713-2745.

Chai, F., S.T. Lindley, J. R. Toggweiler, and R.T. Barber (1999): Testing the importance of iron and grazing in the maintenance of the high nitrate condition in the Equatorial Pacific Ocean, a physical-biological model study. *In: The Changing Ocean Carbon Cycle.* R.B. Hanson, H.W. Ducklow, & J.G. Field (Editors). International Geosphere-Biosphere Programme (IGBP) Book Series 5. Pp. 156-186. Cambridge University Press.

Chai , F., S.T. Lindley and R.T. Barber. 1996. Origin and maintenance of a high NO_3 condition in the equatorial pacific. *Deep Sea Research* II 43: 1031-1064.

Chai, F. (1995): Origin and Maintenance of High Nutrient Condition in the Equatorial Pacific, A Biological-Physical Model Study. Ph.D. dissertation, Duke University, pp170.

Chavez, F.P., K.R. Buck, K.H. Coale, J.H. Martin, G.R. DiTullio, N.A. Welshmeyer, A.C. Jacobson and R.T. Barber. 1991. Growth rates, grazing, sinking and iron limitation of equatorial Pacific phytoplankton. *Limnology and Oceanography* 36 1816-1833.

Chavez, F.P., J. Ryan, S. Liuch-Cota, and M. Niquen (2003): From Anchovies to Sardines and Back – Multidecadal Change in the Pacific Ocean. *Science*, accepted.

Coale, K.H. et al. 1996. A massive phytoplankton bloom induced by an ecosystem-scale iron fertilization experiment in the equatorial Pacific Ocean. *Nature* 838: 495-501.

Conkright, M., T. O' Brien, M., S. Levitus, T.P. Boyer, J. Antonov, C. Stephens (1998): World Ocean Atlas 1998 Vol. 11: Nutrients and Chlorophyll of the Pacific Ocean. NOAA Atlas NESDIS 37.*U.S. Gov. Printing Office, Wash., D.C.*, 245 pp.

da Silva, A.M., C. C.Young-Molling, and S. Levitus, 1994: Atlas of Surface Marine Data 1994, Vol. 1: Algorithms and Procedures. NOAA Atlas NESDIS 6. *U.S. Gov. Printing Office, Wash., D.C.,* 83 pp.

Deser, C., M.A. Alexander, and M.S. Timlin (1996): Upper-Ocean Thermal Variations in the North Pacific during 1970-1991. *Journal of Climate:* Vol. 9, No. 8, 1840-1855.

Denman, K.L. and M A. Pena (1999): A coupled 1-D biological/physical model of the northeast subarctic Pacific Ocean with iron limitation. *Deep Sea Research* II 46: 2877-2908.

Ding, L.-J. and T. Saino (1999): Seasonal and long-term interannual variations of biological environments in Oyashio surface waters off Tohoku prefecture, Japan. In *Proceedings of 1999 Spring Meeting of the Oceanographic Society of Japan*, pp. 156, Oceanographic Society of Japan, Tokyo, Japan.

Dugdale, R.C., R. T. Barber, F. Chai, T.H. Peng, and F.P. Wilkerson (2002): One Dimensional Ecosystem Model of the Equatorial Pacific Upwelling System, Part II: Sensitivity Analysis and Comparison with JGOFS EqPac Data. *Deep-Sea Res. II*, Vol. 49, No. 13-14, 2746-2762.

Emerson, S., S. Meching, and J. Abell (2001): The biological pump in the subtropical North Pacific Ocean: nutrient sources, Redfield ratios, and recent changes. *Glob. Biogeochem. Cyc.*, 15, 535-554.

Favorite, F., A.J. Dodimead, and K. Nasu (1976): Review of the oceanography of the North Pacific, 1960-1971. *Bull. Int. North Pacific Fish. Commun.* 33, 1-187.

Francis, R. C. and S. R. Hare (1994): Decadal-scale regime shifts in the large marine ecosystems of the North-east Pacific: a case for historical science. Fish. Oceanogr. 3: 279-291.

Freeland, H.J., K.Denman, S.S. Wong, F. Whitney and R. Jacques (1997): Evidences of change in the winter mixed layer in the Northeast Pacific Ocean. *Deep-Sea Res*. 44: 21117-2129.

Frost, B.W. and N.C. Franzen. (1992): Grazing and iron limitation in the phytoplankton stock and nutrient concentration: a chemostat analogue of the Pacific equatorial upwelling zone. Marine. *Ecology Progress Series* 83: 291-303.

Frost, B.W. and M.J. Kishi (1999): Ecosystem dynamics in the eastern and western gyres of the Subarctic Pacific a review of lower trophic level modeling. *Progress in Oceanography,* 43, 317-333.

Graham, N.E. (1994): Decadal-scale climate variability in the tropical and North Pacific during the 1970s and 1980s: Observations and model results. Clim. Dyn. 10, 135-162.

Gent, P. and J.C. McWilliam, 1990: Isopycnal mixing in ocean circulation models, *J.Phys. Oceanogr*., **20**, 150-155.

Gent, P.R., F.O. Bryan, G. Danabasoglu, S.C. Doney, W.R. Holland, W.G. Large, and J.C. McWilliams (1998): The NCAR Climate System Model Global Ocean Component. *J. Climate,* 11, 1287-1306.

Haigh, S.P., K.L. Denman, and W.W. Hsieh (2001): Simulation of the planktonic ecosystem response to pre- and post-1976 forcing in an isopycnic model of the North Pacific. *Can. J. Fish. Aquat. Sci., 58, 703-722.*

Harrison, P.J. (2002): Station Papa time series: Insights into ecosystem dynamics. *Journal of Oceanography*, Vol. 58, 259-264.

Holland, W.R., J.J.C. Chow, and, F.O. Bryan (1998), Application of a third-order upwind scheme in the NCAR ocean model. *J. Climate*, **11**, 1487-1493.

Jiang, M-S, F. Chai, R.C. Dugdale, F. Wilkerson, T-H Peng, and R.T. Barber (in revision): A nitrate and silicate budget in the equatorial Pacific Ocean: A coupled biological-physical model study. *Deep Sea Research.*

Karl, D.M., R.R. Bidigae, and R.B. Letelier (2001): Sustained and Aperiodic Variability in Organic Matter Production and Phototrophic Microbial Community Structure in the North Pacific Subtropical Gyre. *In: Phytoplankton Productivity: Carbon assimilation in marine and freshwater ecosystems. P.J. Le B. Williams, D.N. Thomas and C.S. Reynolds (editors). 222-264.* Blackwell Science.

Karl, D.M., R.R. Bidigae, and R.B. Letelier (2001): Long-term changes in plankton community structure and productivity in the North Pacific subtropical gyre: The domain shift hypothesis. *Deep Sea Res*. II, Vol. 48, 1449-1470.

Kawamiya, M. (2002): Numerical model approaches to address recent problems on pelagic ecosystems. *Journal of Oceanography*, Vol. 58, 365-378.

Kawamiya, M., M.J. Kishi, and S. Suginohara (2000a): An ecosystem-physical combined model for the North Pacific. Part 1: Model description and the characteristics of the spatial distributions of biological variables. *J. Mar. Syst*. 25, 129-157.

Kawamiya, M., M.J. Kishi, and S. Suginohara (2000b): An ecosystem-physical combined model for the North Pacific. Part 1I: Mechanisms of the season variation of chlorophyll. *J. Mar. Syst*. 25, 159-178.

Kobayashi, T. (1999): Study of the formation of North Pacific Intermediate Water by a general circulation model and the particle-tracking method 1. A pitfall of general circulation model studies. *Journal of Geophysical Res.,* Vol. 104, No. 3, 5423-5439.

Landry, M R., R.T. Barber, R.R. Bidigare, F. Chai, K.H. Coale, H.G. Dam, M.R. Lewis, S.T. Lindley, J.J. McCarthy, M.R. Roman, D.K. Stoecker, P.G. Verity, J.R. White (1997): Iron and Grazing Constraints on Primary Production in the Central Equatorial Pacific: An EQPAC Synthesis. *Limnol. Oceanogy,* Vol. 42, No.3, 405-418.

Large, W.G., McWilliams, J.C. and Doney, S.C. (1994). Oceanic vertical mixing: a review and a model with a nonlocal boundary layer parameterization. *Review of Geophysics*, 32: 363-403.

Lehodey, P. and F. Chai (submitted): Application of a spatial environmental population dynamics model (SEPODYM) to skipjack (*Katsuwonus pelamis*) and albacore (*Thunnus alalunga*) in the Pacific Ocean. *Fisheries Oceanography.*

Levitus, S; Conkright, ME; Reid, JL; Najjar, and RG; Mantyla (1993): A Distribution of nitrate, phosphate and silicate in the world oceans. *Progress in Oceanography* vol. 31, no. 3, pp. 245-273.

Levitus, S., R. Burgett, T. Boyer (1994): World Ocean Atlas 1994, Vol. 3: Salinity. NOAA Atlas NESDIS 3, *U.S. Gov. Printing Office, Wash., D.C.,* 99 pp.

Levitus, S., T. Boyer (1994): World Ocean Atlas 1994, Vol. 4: Temperature. NOAA Atlas NESDIS 4, *U.S. Gov. Printing Office, Wash., D.C.,* 117 pp.

Li, X., Chao, Y., McWilliams, J.C. and Fu, L.-L., 2001. A comparison between two vertical mixing schemes in a Pacific OGCM. *Journal of Climate*, Vol. 14, No. 7, 1377-1398.

Limsakul, A., T. Saino, T. Midorikawa and J.I. Goes (2001): Temporal variations in lower trophic level biological environments in the northwestern North Pacific Subtropical Gyre from 1950 to 1997. *Progress in Oceanography,* 49,129-149.

Longhurst, A. (1998): *Ecological Geography of the Sea*. Pp. 391. Academic Press, San Diego.

Lynn, R.J. (1986): The subarctic and northern subtropical fronts in the eastern North Pacific Ocean in spring. *Journal of Physical Oceanography*, 16, 209-222.

Maldonado, M.T., P.W. Boyd, P.J. Harrison, and N.P. Price (1999): Co-limitation of phytoplankton growth by light and Fe during winter in the subarctic Pacific Ocean. *Deep-Sea Res. II*, 46, 2475-2485.

Mantua, N. J., S. R. Hare, Y. Zhang, J.M. Wallace, and R.C. Francis (1997): A Pacific interdecadal climate oscillation with impacts on salmon production. *Bull. Am. Meteor. Soc*. 78:1069-1079.

Mantua, N.J. and S.R. Hare (2002): The Pacific Decadal Oscillation. *Journal of Oceanography*, Vol. 58, 35-44.

Martin, J.H., G.A. Knauer, D.M. Karl and W.W. Broenkow, 1987, VERTEX: carbon cycling in the northeast Pacific. *Deep-Sea Res*, **34**(2), 267-285.

Martin, J.H. and S.F. Fitzwater (1988): Iron deficiency limits phytoplankton growth in the north-east Pacific subarctic. *Nature*, 331, 341-343.

McGowan, J. A., D. R. Cayan, and L. M. Dorman (1998): Climate-ocean variability and ecosystem response in the northeast Pacific. *Science, 281,* 210-217.

Miller, A. J., D. R. Cayan, T. P. Barnett, N. E. Graham and J. M. Oberhuber, 1994: The 1976-77 climate shift of the Pacific Ocean. *Oceanography, 7,* 21-26.

Miller, A. J. and N. Schneider (2000): Interdecadal climate regime dynamics in the North Pacific Ocean: Theories, observations and ecosystem impacts. *Progress in Oceanography*, 47, 355-379.

Miller, A.J., M.A. Alexander, G.J. Boer, F. Chai, K. Deman, D.J. Erickson, R. Frouin, A.J. Gabric, E.A. Laws, M.R. Lewis, Z. Liu, R. Murtugudde, S. Nakamoto, D.J. Neilson, J.R. Norris, J.C. Ohlmann, R. Perry, N. Schnerider, K. Shell, and A. Timmermann (2003): Potential Feedbacks Between Pacific Ocean Ecosystems and Interdecadal Climate Variations. Bulletin of the American Meteorological Society, in press.

Minobe, S. (1999): Resonance in bidecadal and pentadecadal climate oscillations over the North Pacific: Role in climatic regime shifts. *Ceophys. Res. Lett., 26,* 855-858.

Monterey, G.I., and Levitus, S. (1997): Seasonal Variability of Mixed Layer Depth for the World Ocean. NOAA NESDIS Atlas 14*, U.S. Gov. Printing Office, Wash., D.C.,* 5 pp. 87 figs.

Ono, T., T. Midorikawa, Y. W. Watauabe, K. Tadokoro, and T. Saino (2001): Temporal increases of phosphate and apparent oxygen utilization in the subsurface waters of western subarctic Pacific from 1968 to 1998. *Geophys. Res. Lett.,* 28, 3285-3288.

Pacanowski, R., K. Dixon and A. Rosati (1991): The GFDL modular ocean model users guide, version 1.0. Tech. Rep. 2, Ocean Group, Geophys. Fluid Dyn. Lab., Princeton.

Polovina, J.J., G. T. Mitchum, N. E. Graham, M. P. Craig, E. E. DeMartini, and E. N. Flint (1994): Physical and biological consequences of a climatic event in the Central North Pacific. *Fish. Oceanogr.,* 3, 15-21.

Polovina, J.J., G. T. Mitchum, and G. T. Evans (1995): Decadal and basin-scale variation in mixed layer depth and the impact on biological production in the Central and North Pacific, 1960-88. *Deep Sea Res*. 42: 1701-1716.

Polovina, J.J., D.R. Kobayashi, D.M. Parker, M.P. Seki, and G.H. Balazs (2000): Turtles on the edge: movement of loggerhead turtles (*Caretta caretta*) along oceanic fronts spanning longline fishing grounds in the central North Pacific, 1997-1998. *Fisheries Oceanography*, 9, 1-13.

Polovina, J.J., E. Howell, D.R. Kobayashi, M.P. Seki (2001): The transition zone chlorophyll front, a dynamic global feature defining migration and forage habitat for marine resources. *Progress in Oceanography*, 49, 469-483.

Ragueneau, O., P. Treguer, A. Leynaert, R.F. Anderson, M.A. Brzeinski, D. J. Demaster R.C.Dugdale et al., 2000, *Global and Planetary Change*, **26**: 317-365.

Roden, G.I. (1991): Subarctic-subtropical transition zone of the North Pacific: large-scale aspects and mesoscale structure. In J.A. Wetherall (ed.), *Biology, oceanography and fisheries of the North Pacific Transition Zone and Subarctic Frontal Zone* (pp. 1-38). NOAA Technical Report. NMFS 105.

Suga, T., A. Kato, and K. Hanawa (2000): North Pacific tropical water: its climatology and temporal changes associated with the climate regime shift in the 1970s. *Journal of Oceanography*, 47, 223-256.

Sugimoto, T., and K. Tadokoro (1997): Interannual-interdecadal variations in zooplankton biomass, chlorophyll concentration and physical environment in the subarctic Pacific and Bering Sea. *Fish. Oceanogr.,* 6, 74-93.

Trenberth, K. E. and J. W. Hurrell (1994): Decadal atmosphere-ocean variations in the Pacific. *Clim. Dyn*. 9: 303-319.

Venrick, E. L., J. A. McGowan, D. R. Cayan, and T. L. Hayward (1987): Climate and chlorophyll a: long-term trends in the central north Pacific Ocean. *Science*, 238: 70-72.

Wefer, G. 1989. Particle flux in the ocean: effects of episodic production. In: Productivity of the ocean; Present and past. W.H. Berger, V.S. Smetacek, and Wefer (Eds.) Dahlem workshop reports, 44. Pp. 85-98.

Wong, C.S, N.A. Waser, Y. Nojiri, W.K. Johnson, F.A. Whitney, J.S. Page, and J. Zeng (2002): Seasonal and interannual variability in the distribution of surface nutrients and dissolved inorganic carbon in the Northern North Pacific: influence of El Nino. *Journal of Oceanography*, Vol. 58, 227-243.

Xie, S.-P., T. Kunitani, A. Kubokawa, and S. Hosoda (2000): Interdecadal thermocline variability in the North Pacific for 1958-97: A GCM simulation. *J. Phys. Oceanogr*. 30, No. 11, 2798-2813.

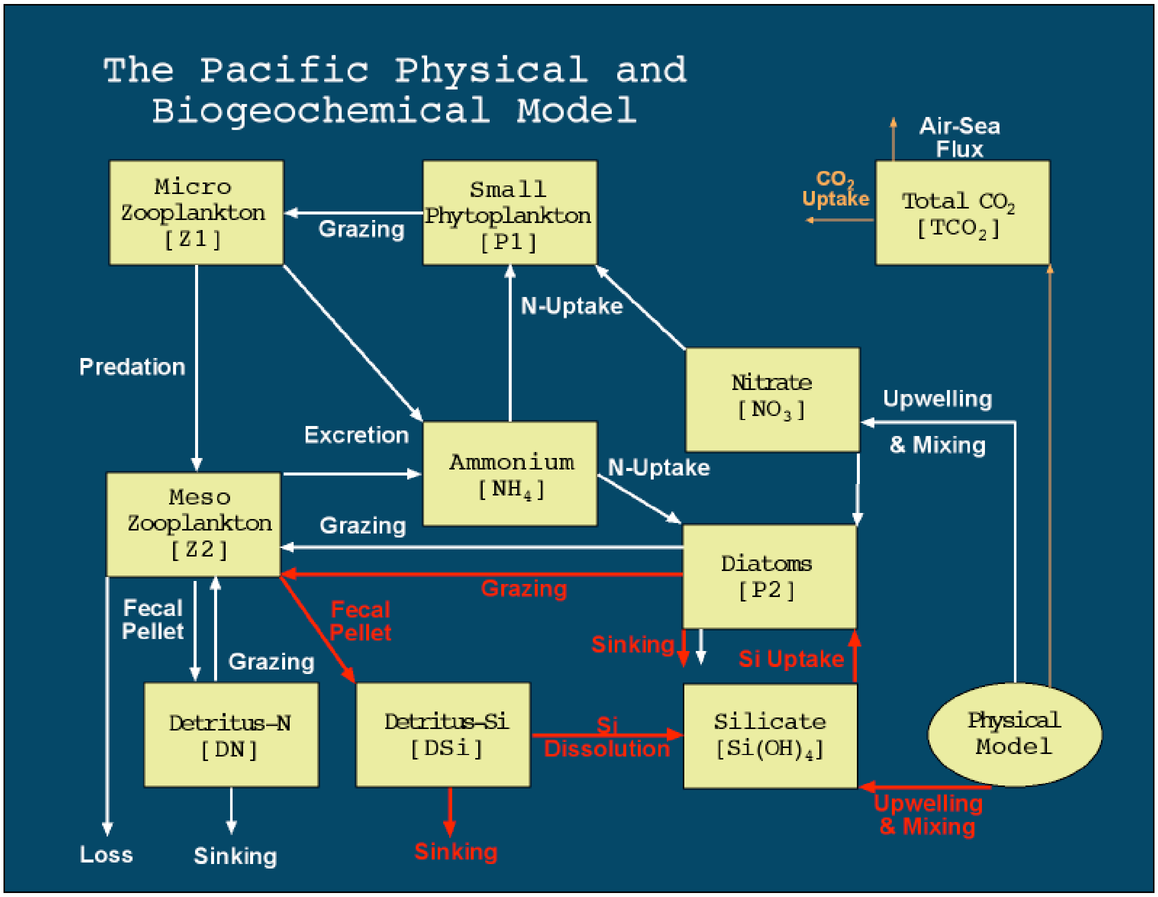

Figure 1: The inter-compartmental flow chart of the ecosystem and linkage to carbon and physical processes in the euphotic zone. The flow of nitrogen is indicated by solid line; the flow of silicon is indicated by dashed line; and the carbon flow is indicated by line-dashed line.

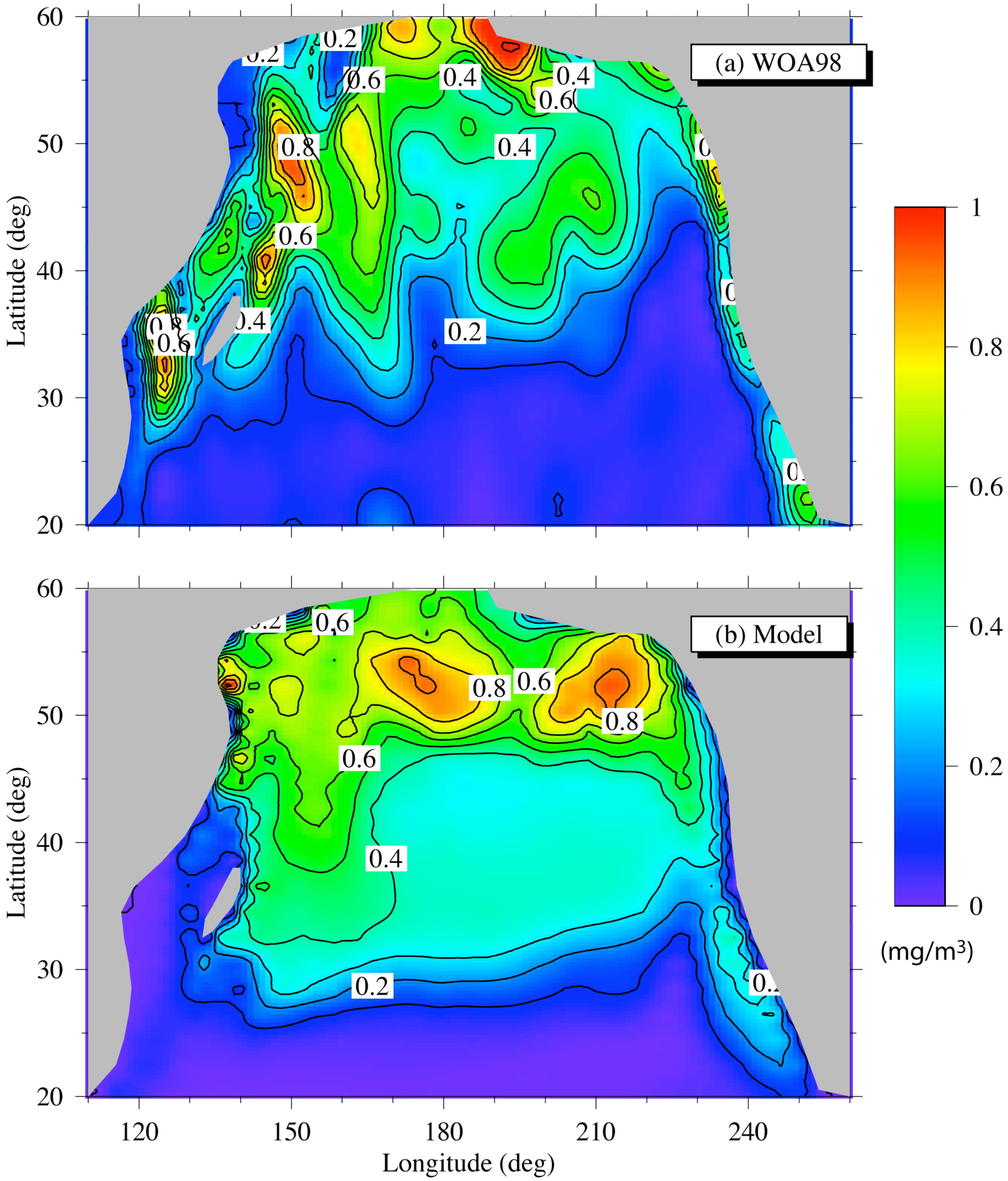

Figure 2: Comparisons of the modeled surface chlorophyll and WOA98 data in spring (April-May-June) (unit: mg/m^3). The modeled surface chlorophyll concentration was derived from the modeled top layer (5 m) phytoplankton biomass concentration (mmol N/m^3), that was converted to mg/m^3 using a nominal gram chlorophyll to mole nitrogen ratio of 1.58, which corresponds to a chlorophyll to carbon mass ratio of 1:50 and a C:N mole ratio of 6.625.

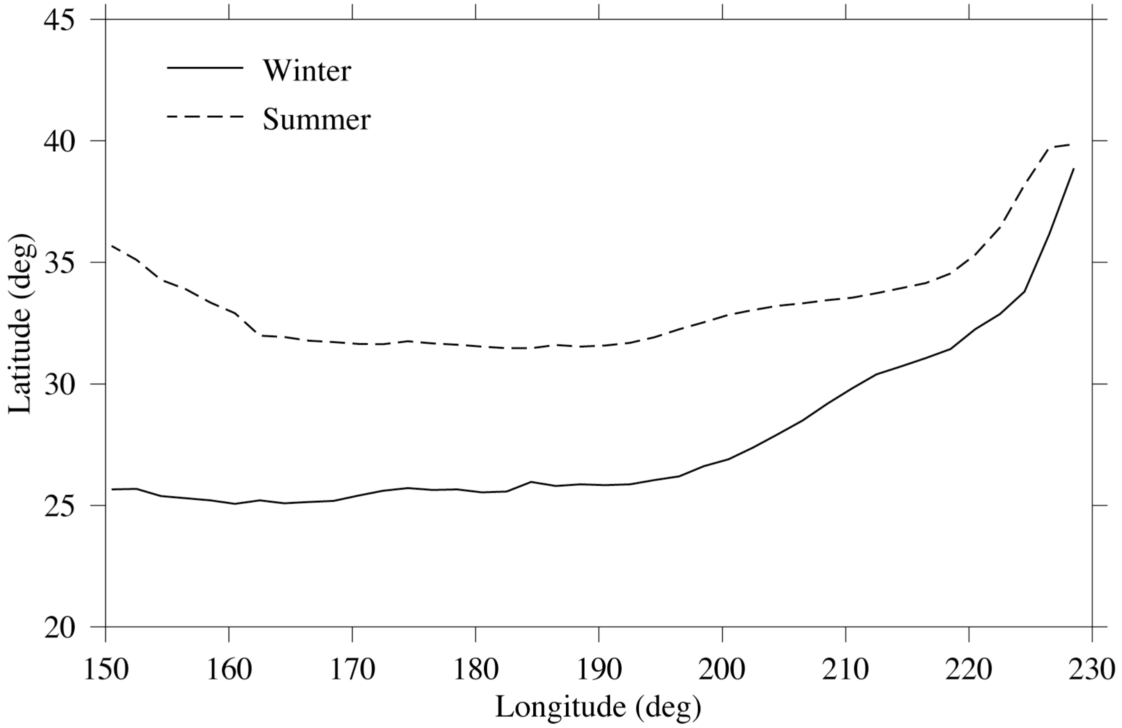

Figure 3: The locations of the transition zone chlorophyll front (chlorophyll = 0.2 mg/m^3) during the climatological winter (January-February-March) and summer (July-August-September).

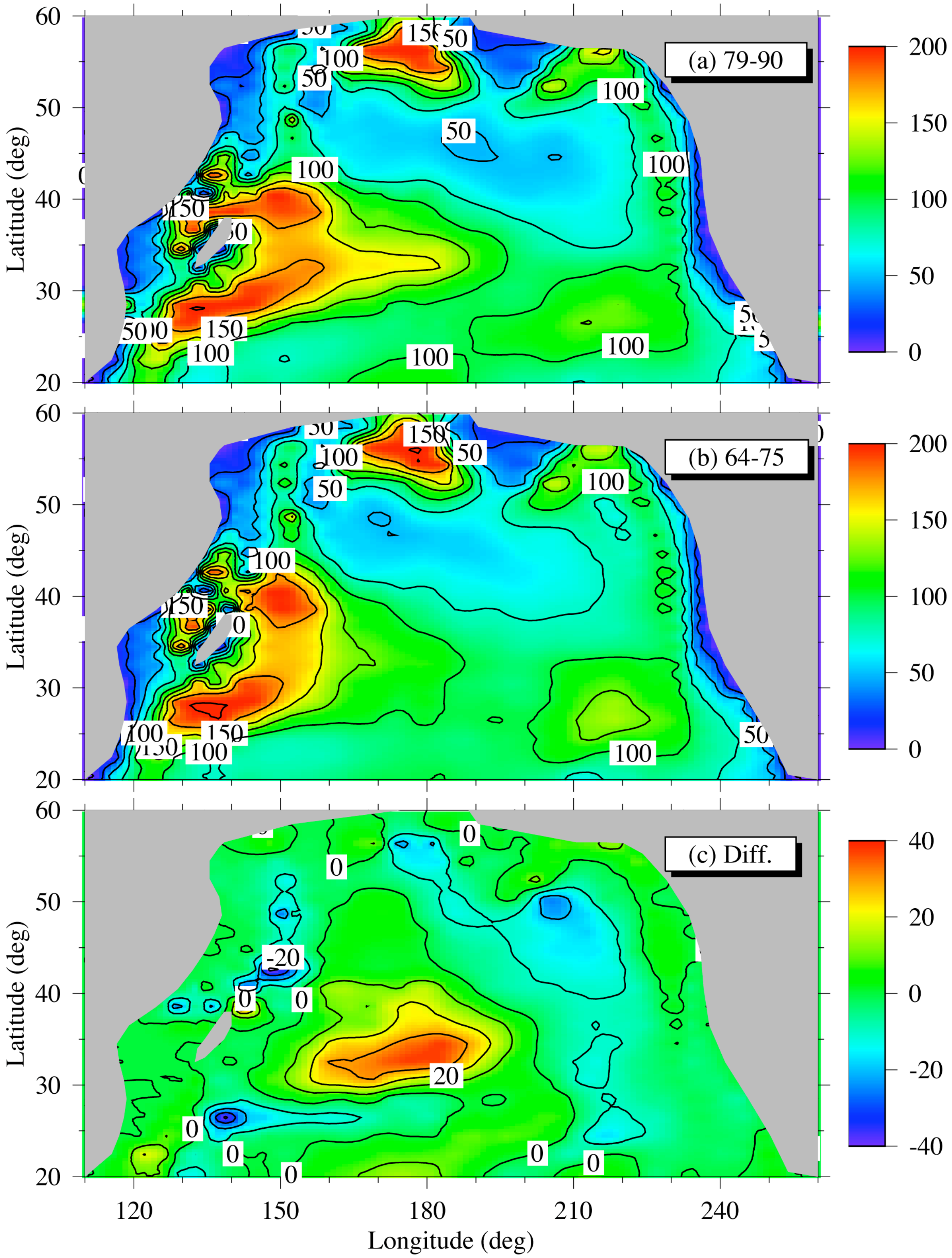

Figure 4: The modeled winter (January-February-March) mixed layer depth (meters) during the period of 1970-90 (a) and 1964-75 (b). The difference (a-b) between 1979-90 and 1964-75 (c). In (c), position values mean deeper MLD, for example, 20 equals 20 meters deeper in the MLD.

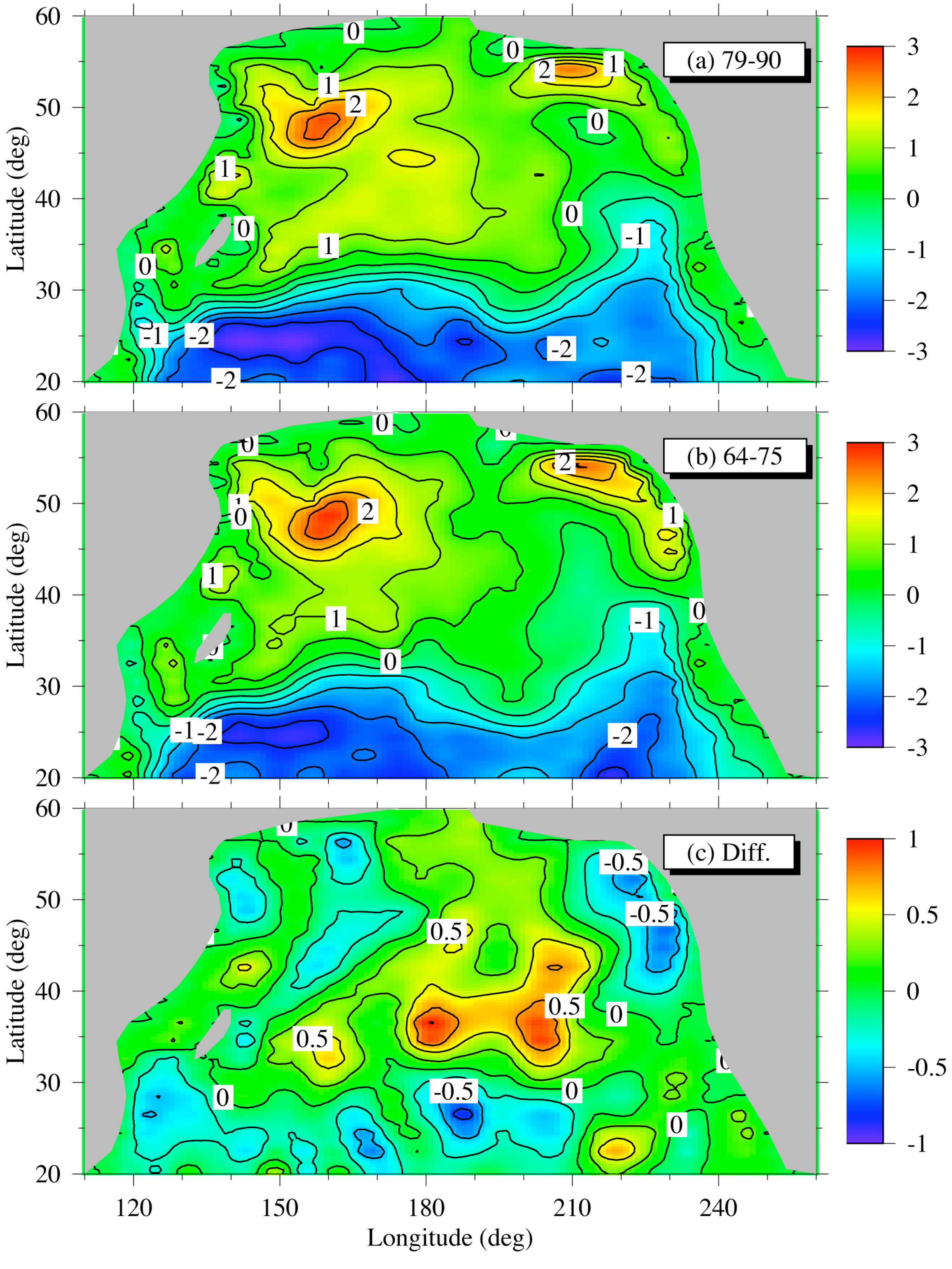

Figure 5: The winter (January-February-March) Ekman pumping velocity (1 X 10^{-6} m/sec) during the period of 1979-90 (a) and 1964-75 (b), the positive is upward motion. The difference (a-b) between 1979-90 and 1964-75 (c). In (c), positive values mean stronger Ekman pumping velocity.

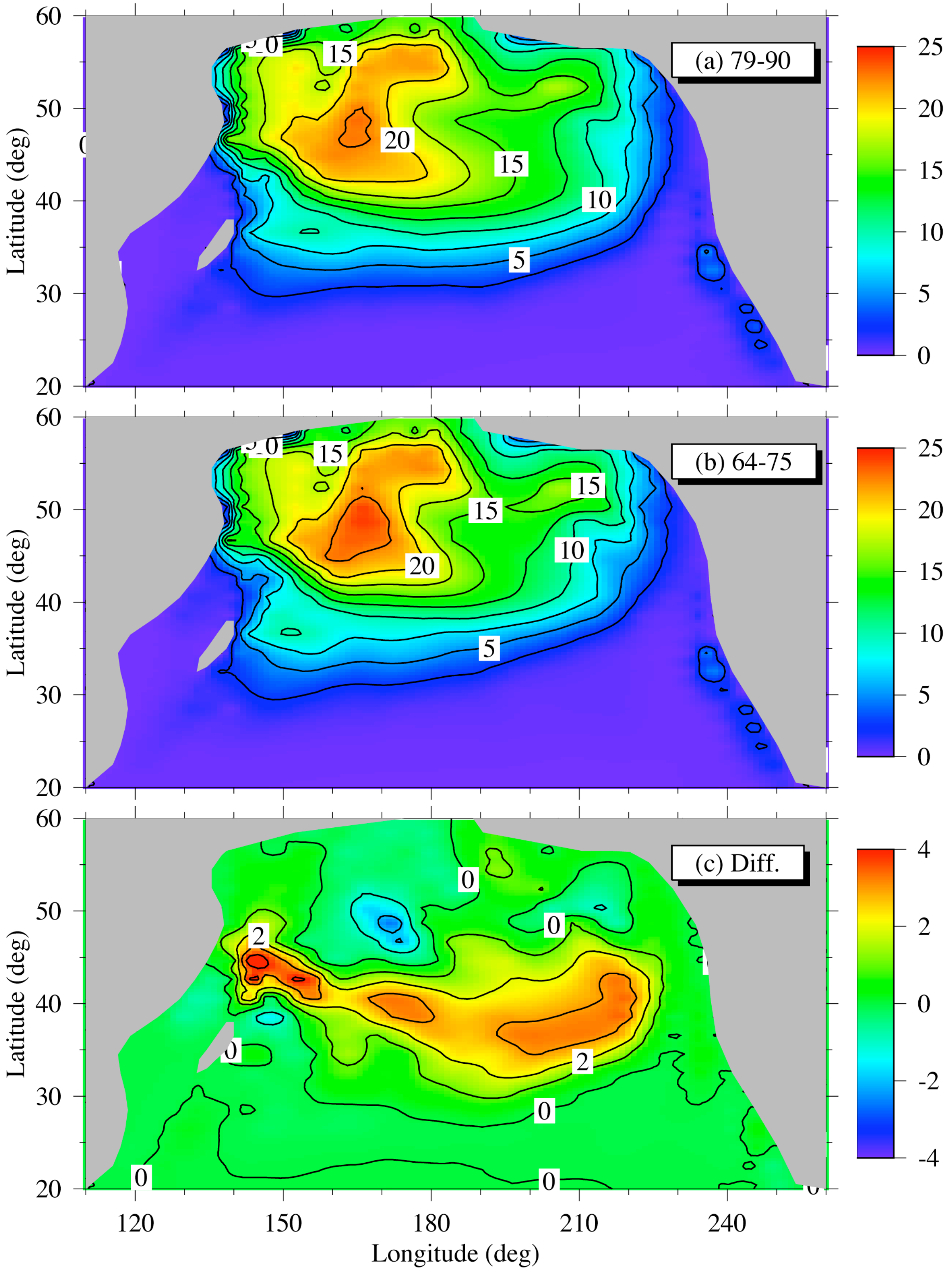

Figure 6: The modeled winter (January-February-March) surface nitrate concentration (mmol/m^3) during the period of 1979-90 (a) and 1964-75 (b). The difference (a-b) between 1979-90 and 1964-75 (c). In (c), positive values mean increase in the surface nitrate concentration.

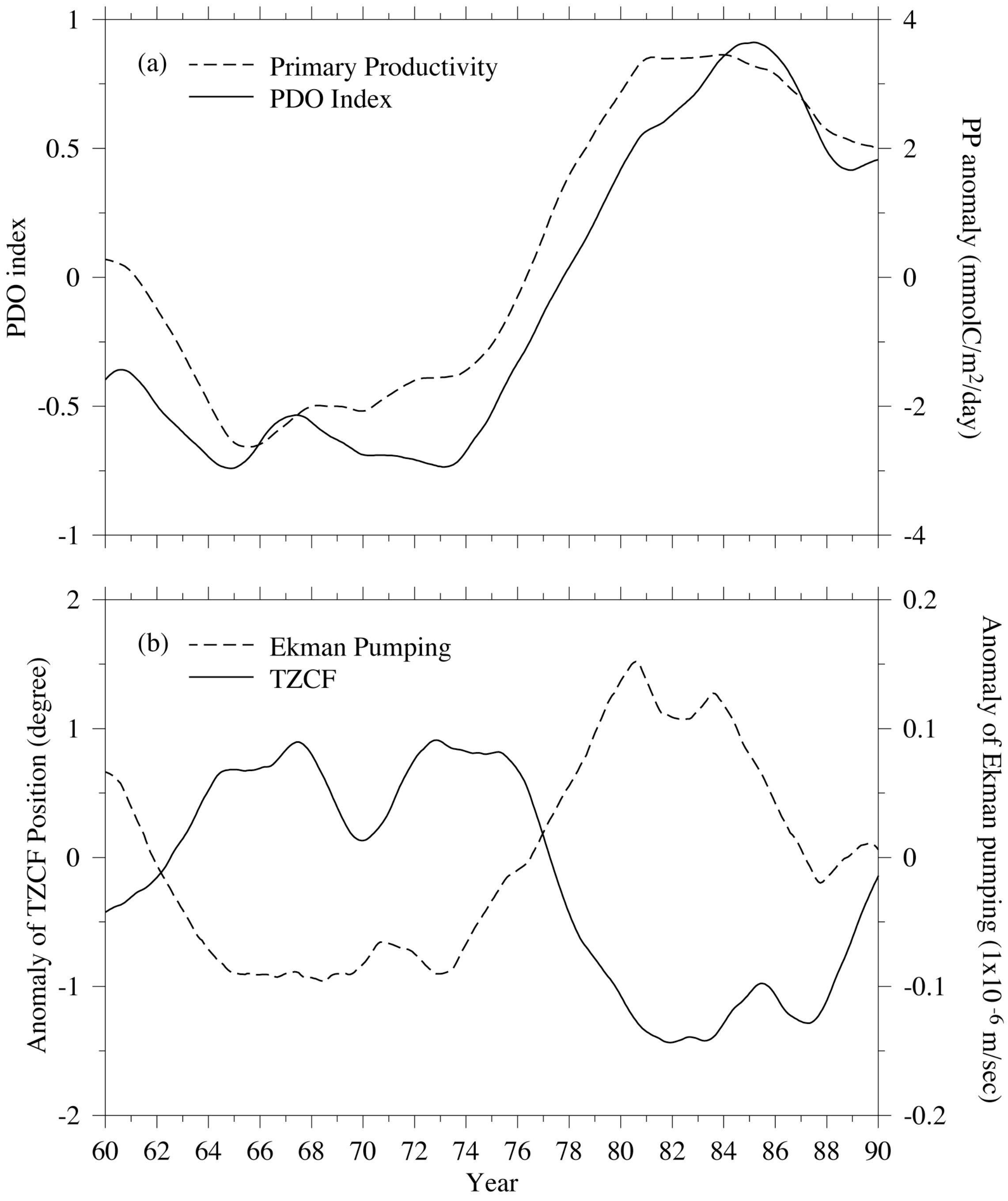

Figure 7: (a) PDO index and primary production (PP) anomaly in the central North Pacific (30^{o}N-40^{o}N and 180^o-140^{o}W). The PDO Index is defined as the leading principal component of North Pacific monthly sea surface temperature variability (poleward of 20^{o}N for the 1900-93 period), see http://tao.atmos.washington.edu/pdo/ for more details (Mantua and Hare, 2002), courtesy of Dr. Nathan Mantua at University of Washington. The monthly averaged PP anomaly was derived by removing the seasonal cycle (it includes all seasons, not just winter time). Both PDO and PP anomaly were smoothed with 7 year and 2 year running mean filters. (b) The anomaly of Ekman pumping velocity in the central North Pacific and TZCF (chlorophyll = 0.2 mg/m^3) anomaly (latitudinal, in degree) averaged between 180^o-140^{o}W. Again, both anomalies were derived by removing

seasonal cycles and then smoothed with the same running filters as in (a). It includes all the seasons, not just the winter time. The positive anomaly means the TZCF moves northward, and negative anomaly means the equatorward movement.